Post-Print

Submitted, accepted and published in
Applied Catalysis A: General 456 (2013) 88-95

Synthesis and application of gold-carbon hybrids as catalysts for the hydroamination of alkynes

Andrés Seral-Ascaso [a,b], Asunción Luquin [b], María Jesús Lázaro [a], Germán F. de la Fuente [c], Mariano Laguna [b], Edgar Muñoz [a,*]

[a] Instituto de Carboquímica ICB-CSIC, Miguel Luesma Castán 4, 50018 Zaragoza, Spain

[b] Instituto de Síntesis Química y Catálisis Homogénea (Universidad de Zaragoza-CSIC), Plaza San Francisco s/n, 50009 Zaragoza, Spain

[c] Instituto de Ciencia de Materiales de Aragón (Universidad de Zaragoza-CSIC), María de Luna 3, 50018 Zaragoza, Spain

[*]Corresponding author at: Instituto de Carboquímica ICB-CSIC, Miguel Luesma Castán 4, 50018 Zaragoza, Spain. Tel.: +34 976 733977; fax: +34 976 733318.

E-mail Address: edgar@icb.csic.es (E. Muñoz).

ABSTRACT

Gold-carbon hybrids have been efficiently used as catalysts for the hydroamination of phenylacetylene with aniline. Carbon supports (single-walled and multi-walled carbon nanotubes, graphene oxide, graphite, graphitic cones, nanodiamond, ordered mesoporous carbon, carbon xerogel, carbon black, activated carbon, and laser-ablation produced carbon foam) were homogenously decorated with gold nanoparticles (GNP) synthesized by *in situ* reduction of chloroauric acid ($H[AuCl_4]$) in water. The performance of carbon materials used as catalytic supports has been here evaluated. The synthesized gold-carbon hybrids worked remarkably well as catalysts for the targeted reaction. Conversion values as high as 79 % were achieved by suitably adjusting the gold:carbon support w/w ratios. Our results indicate that the catalytic activity strongly depends on gold:carbon support w/w ratios and on the structure and textural properties and dispersibility of the carbon supports used. Thus, the best gold-carbon catalyst performance in terms of conversion values and low carbon support content has been achieved when using graphene oxide as well as supports (carbon black, carbon nanotubes, and nanodiamond) that combine high BET surface areas, well-developed mesoporosity, and good dispersibility in water during the GNP decoration process.

Keywords: Gold-carbon catalysts; gold nanoparticles; hydroamination; carbon supports; gold-carbon hybrids

1. Introduction

Metal nanoparticle decoration is able to provide fascinating catalysis application opportunities to carbon materials. Thus, applications for these metal-carbon hybrids have been successfully demonstrated in fuel cell technologies [1-4] and heterogeneous catalysis [5-9]. On the other hand, the use of gold nanoparticle (GNP)-based catalysts has been widely explored in recent years [10]. Hence, while the bulk metal is largely non-active in catalysis [11], GNP exhibit a surprisingly high catalytic activity, which mainly depends on the nanoparticle size and the support used [12-15]. Additionally, GNP-based catalysts enable operating at low reaction temperatures and, in most cases, provide high reaction selectivity [15,16]. GNP-decorated carbon supports are able to provide outstanding catalytic performance [17-21]. Eventually, the catalytic performance of the deposited GNP may be synergistically favored by the carbon supports used [17,19,22,23]. A variety of methods are being utilized for the synthesis of gold-carbon hybrids [24,25], including physicochemical methods such as electrodeposition [26] or laser ablation of metal targets in liquids [27], and the most commonly used wet chemical strategies involving the reduction of gold containing compounds [22, 28].

Hydroamination reactions enable the synthesis of nitrogen-containing organic compounds which are widely present in the nature and provide biological- and pharmaceutical activity [29], and can be used in cosmetics as well as intermediates in many industrial processes and in the synthesis of agrochemical products [30]. The conventional synthesis routes to obtain C-N bond-containing molecules are however limited, hence it is of great importance the development of methods to catalytically add a nucleophile nitrogen to a C-C multiple bond [31,32]. Gold-containing complexes and

GNP are able to efficiently catalyze this reaction [33,34]. Moreover, the use of GNP in the catalysis of hydroamination reactions avoids the use of acidic media and the formation of by-products in very regioselective hydroamination reactions [11,35].

In this work we show that carbon materials of a variety of structural, textural, composition and dispersibility properties could be efficiently used as supports for GNP-based catalysts. Thus, different carbon supports - graphene oxide (GO), single-walled carbon nanotubes (SWCNT), multi-walled carbon nanotubes (MWCNT), graphitic cones (GC), graphite (G), nanodiamond (ND), carbon xerogel (CX), carbon black (CB), activated carbon (AC), ordered mesoporous carbon (OMC), and laser-ablation-produced nanostructured carbon foam (CF)- have been chemically decorated with GNP, and the resulting gold-carbon hybrids have been then tested for the catalysts of the hydroamination of phenylacetylene with aniline [35]. Scheme 1 shows the reaction pathway proposed by Corma et al. by which the hydroamination of phenylacetylene with aniline occurs through the regioselective Markovnikov rule to yield an enamine that, subsequently, tautomerizes to the more stable imine (phenyl-(1-phenylethilidene)amine) [35].

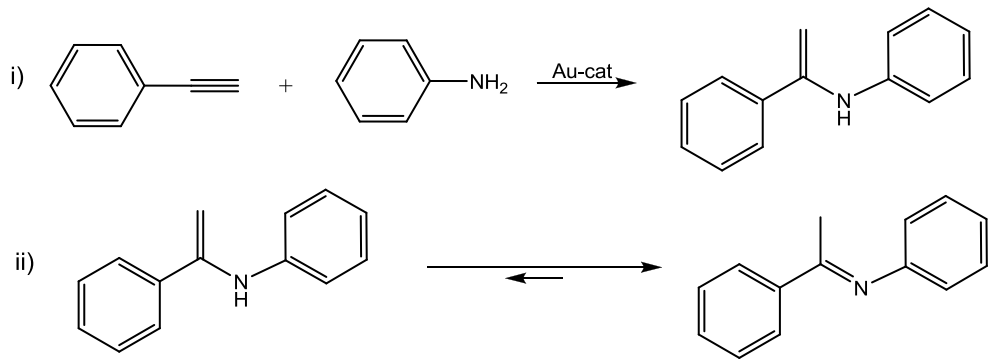

Scheme 1. Au-assisted catalysis of the hydroamination of phenylacetylene with aniline [35].

Conversion values of up to 79 % have been achieved with the synthesized gold-carbon hybrids. Our results indicate that the measured catalytic performance strongly depends on the carbon support used as well as on the gold:carbon support w/w ratios.

2. Experimental

Commercial carbon materials, including SWCNT produced by the high-pressure CO disproportionation technique (as-produced HiPco SWCNT [36], Carbon Nanotechnologies Inc., batch# RO501), high purity MWCNT produced by the CVD technique (10-15 nm in diameter, ≥ 10 microns in length, Nanothinx S.A.), single layer GO (CheapTubes Inc.; purity: 99 %. wt., synthesized by a modified Hummers' method [37]), GC produced by hydrocarbon pyrolysis (n-TEC) [38], G (Merck, particle size <50 μm), Vulcan XC-72R CB (Delta Tecnic S.A.), ND (purified, grade G01, PlasmaChem), and AC (Morgui Clima S.L.) were here tested as carbon supports. Our study also includes CX prepared by polycondensation of resorcinol and formaldehyde in water by Pekala's sol-gel method [39], OMC synthesized using a template-mediated process described elsewhere [1], and CF, a nanostructured carbon material that consists mainly of aggregates of amorphous carbon nanoparticles produced by laser ablation of naphthalene [40].

Elemental analysis (Thermo Flash EA 1112 Series NC analyzer) data of the carbon supports used are shown in Table 1. All tested carbon materials have carbon contents over 80 wt. %, except GO due to its high oxygen content (44.9 wt.%) and SWCNT because of the ~20 wt. % Fe catalyst that resulted of the HiPco SWCNT

production process [36], as determined by thermogravimetric analysis (TGA, Setaram Setsys 2000 thermobalance, samples were analyzed in Pt pans at a heating rate of 10ºC/min up to 850ºC in an atmosphere of air flowing at 100 mL/min). The selected carbon supports exhibit significant differences in textural properties, as shown in Table 2. Nitrogen adsorption–desorption isotherms were measured at 77 K (Micromeritics ASAP 2020). Surface area measurements and porosity were studied using the Brunauer–Emmett–Teller (BET) method between 0.05 and 0.3 P/P_0, and t-Plot and Barret-Joyner-Halenda (BJH) methods.

GNP decoration of carbon materials was performed by *in situ* reduction of chloroauric acid ($H[AuCl_4]$, Sigma-Aldrich, 99.999 %) with sodium citrate (Sigma-Aldrich, 99.0 %) and sodium borohydride ($NaBH_4$, Sigma-Aldrich, 98 %) in water [41,42] as follows: the carbon supports were dispersed in 25 mL of a 5.4 mM sodium citrate aqueous solution, and then bath-sonicated for 2 hours. The resulting carbon dispersions were subsequently transferred to a boiling flask, followed by the addition of 23 mL of distilled water. The dispersion was refluxed and 2 mL of a 12.5 mM $H[AuCl_4]$ solution were poured to the boiling dispersion. Then, 100 µL of a freshly prepared 112 mM $NaBH_4$ solution were added. $NaBH_4$ is a strong reducing agent broadly used to produce small GNP, and it is here utilized to boost the full reduction of $H[AuCl_4]$ [43-45]. It is then assumed that under these experimental conditions the reduction from Au(III) to Au(0) was complete. The mixture was kept at 100 ºC until the GNP decoration process ended. The duration of this process depends of the decorated carbon support: 30 minutes for SWCNT, MWCNT and CB, 4 hours for CF and GC, and 12 hours for the rest of carbon supports tested. This suggests that certain characteristics and compositions of the carbon supports used may ease the GNP decoration process. Fixed $H[AuCl_4]$, sodium citrate, and $NaBH_4$ concentrations were utilized in all GNP

decoration experiments. Contrary to the formation of GNP directly on MWCNT sidewalls described by Zhang et al. [28], this *in-situ* decoration process leads to the formation of GNP in solution, that then adhere to the carbon supports. In absence of carbon supports, UV-vis characterization (Thermo Scientific Evolution 600 spectrometer) of the resulting red wine colored GNP solutions shows the characteristic GNP surface plasmon resonance band at 525 nm [46]. The time required for GNP incorporation onto the carbon supports used and, therefore, the efficiency of this chemical GNP decoration method can be monitored by measuring the evolution of UV-vis spectra of solutions that result of filtering the synthesized gold-carbon hybrids, so the 525 nm band is no longer observed when complete GNP decoration is finally reached.

The gold/carbon support dispersions were then cooled down to room temperature, filtered through a 0.22 μm polycarbonate membrane filter (Millipore, GTTP02500), and washed (3x10 mL water, and 3x10 mL acetone) to remove solvent- and reactant traces and, eventually, non-attached GNP. Finally the resulting gold-carbon hybrids were dried in an oven at 110 ºC for 1 hour. The effect of adjusting the gold:carbon support w/w ratios used (i.e. the gold loading of the resulting gold-carbon hybrids) for this GNP decoration procedure was studied for each carbon support for the catalysis application mentioned above.

GO required a modified GNP decoration process to prevent that the material becomes largely agglomerated during filtration, which would hinder its subsequent use in catalysis. Thus, after 12 h of decoration, Au/GO suspensions were filtered until 1 mL of the initial dispersion was left. The material was then redispersed by sonication and finally washed (3x10 mL water, and 3x10 mL acetone) and partially filtered, so the Au-

GO material was kept in ~1 mL acetone prior to proceeding with the catalysis experiments.

The resulting gold-carbon hybrids were characterized by transmission electron microscopy (TEM, JEOL JEM 2000 FXII microscope, operated at 60 kV, equipped with a CCD GATAN mod. 609 camera), TGA, and X-ray diffraction (XRD, CuK_{α} radiation, Bruker D8 Advance Series 2). The average Au fcc crystallite size of GNP was calculated from XRD measurements using the Scherrer equation [47].

The hydroamination of phenylacetylene with aniline was used here to test the catalytic activity of the synthesized gold-carbon hybrids. The reaction was carried out in air atmosphere and using anhydrous solvents to avoid the formation of acetophenone, which can be easily obtained as by-product in presence of water under these conditions [35]. The hydroamination reaction was performed in a 15 mL Schlenk tube equipped with a magnetic stirrer. In a typical experiment, the gold-carbon hybrids were redispersed in deuterated toluene (1 mL; 99.8 at. % D, anhydrous, Sigma-Aldrich) inside a Schlenk tube by mild (bath) sonication. The starting gold content was 2.5 mol % with respect to the reactants in all experiments. Subsequently, aniline (93 mg, 1 mmol; purity >99.5 %, Fluka), phenylacetylene (102 mg, 1 mmol; purity >98 %, Panreac) were added to the suspension. The reaction mixture was then placed in an oil bath at 100 ºC for 24 h.

After reaction, the resulting dispersion was filtered through a celite filter, and the filtrate was analyzed by quantitative ^{1}H NMR (Bruker AV 400 spectrometer) using dodecane as internal standard (47 mg, 0.25 mmol; purity >99.8 %, Sigma-Aldrich). Calibration was used to follow the course of the reaction. The conversion was calculated referred to the dodecane signal at 1.31 ppm. The reactants reference signals were those of the aniline appearing between 6.17 and 6.44 ppm, and those assigned to

phenylacetylene at a chemical shift between 7.28 and 7.45 ppm. For the reaction product, the signal used to calculate the conversion was the one at 1.88 ppm. Again, the use of GO supports required a modified procedure: 1 mL Au-GO hybrid acetone dispersion samples were carefully transferred to a Schlenk tube and mixed with 4 mL of deuterated toluene. The mixture was stirred and then heated to 80 ºC while bubbling with dry air to remove acetone. The complete acetone removal was confirmed by ^{1}H NMR.

3. Results and Discussion

TEM characterization reveals that efficient GNP decoration of all tested carbon supports has been achieved with the chemical method used (Fig. 1 and 2). TEM and XRD characterization indicate that the GNP size strongly depends on the gold:carbon support w/w ratio of the synthesized gold-carbon hybrids and on the structure and dispersibility of the carbon supports.

The application of the synthesized gold-carbon hybrids as catalysts of the hydroamination of phenylacetylene with aniline has been then evaluated. We firstly confirmed that the pristine carbon supports did not provide any catalytic activity. This is an important issue as some of them contain significant amounts of metal nanoparticles or metal traces (most notably, the as-produced HiPco SWCNT used), while others (such as ND) are reported to eventually provide catalytic activity by themselves [48]. On the contrary, the synthesized gold-carbon hybrids act as good catalysts of the investigated organic reaction: Fig. 3 shows the conversions achieved for each gold-carbon hybrid at different gold:carbon support w/w ratios. ^{1}H NMR results discarded the formation of

by-products, therefore indicating the high selectivity of the targeted hydroamination reaction. When suitably adjusting the gold:carbon support ratios, conversion values higher than 60% have been achieved for almost all the tested carbon supports after 24 h reaction, reaching maximum conversion values for CB (79 %), GO (76 %) and MWCNT and SWCNT (74 %, Fig. 3 and Table 3). It is also interesting to point out that GO provided this high conversion values at the lowest carbon support content (Au-GO 1:1) of all decorated carbon materials. For each carbon support tested, the highest conversion values were reached when the complete GNP loading occurs at the lowest carbon support contents. UV-vis spectra of the solutions that result of filtering the gold/carbon support dispersions after GNP decoration and TGA analysis of the synthesized gold-carbon hybrids were used to determine the gold:carbon support compositions that lead to the complete Au loading onto the carbon supports. Thus, as an example, UV-vis studies revealed that all produced GNP are allocated on CB for CB contents $\geq$ 1:2 Au-CB. Therefore, 2:1 Au-CB hybrids were produced in defect of carbon support, as indicated by the deep red wine colored solutions obtained after filtration of the produced Au-CB hybrids. This was further confirmed by TGA analysis, which revealed that only 63% of the starting Au was incorporated as GNP onto CB for this hybrid composition. Increasing the CB content to 1:2 Au-CB however led to the complete GNP decoration of CB. Further increasing the carbon support content hinders the reactants diffusion and, therefore, leads to decreased conversion values. Turnover number (TON) values of up to 40 would be ideally expected for Au catalyst concentration of 2.5 mol %. TON values of around 25-30 were measured for all tested gold-carbon hybrids (Table 3).

The measured GNP average crystallite size that provides the maximum conversion values strongly depends on the carbon support used (Table 3). The smallest

average Au fcc crystallite size values (5.4 to 6.7 nm) were measured for ND and nanostructured mesoporous carbon supports whose structure consists of aggregates of amorphous carbon nanoparticles (CB and CF). The use of graphene-based supports (GC, SWCNT, MWCNT, G, and GO) led to the formation of GNP of larger average Au fcc crystallite size (7.9 to 14.8 nm).

The small GNP size values measured when using CB, ND and CF can be explained in terms of the large number of defects in their structure that would act as anchor points [49], therefore limiting the increase in nanoparticle size that occurs during further agglomeration of GNP before they stick onto the support [28]. Thus, the defective structure of CX is expected to provide small GNP sizes in the synthesized Au-CX hybrids. Instead, values of 14.7 nm were measured in the Au-CX hybrid that provided the best catalytic performance. Additionally, the total amount of CX that must be added to efficiently allocate all synthesized GNP is larger than it would be expected for a material whose BET surface area is larger that those of CB, ND, and CF (Table 2). A careful study of our results indicate that there is a correlation between the dispersibility of the carbon supports, their microporous and mesoporous nature and the obtained GNP size and, therefore, the catalytic performance of the resulting gold-carbon hybrids. Thus, while CF, CB, and ND are mainly mesoporous materials (Table 2), CX exhibits both high micro- and mesoporosity. As mentioned above, sodium citrate acts as a reducing agent, pH buffer and as a surfactant agent not only for GNP but also for the carbon supports in water, enabling their efficient dispersion. Therefore, carbon supports and GNP actually compete for the free citrate available in solution, so for fixed sodium citrate concentration conditions, this citrate concentration available in GNP growth greatly determines the GNP size. Both micropores and mesopores are accessible for small molecules like citrate, so the use of carbon supports of large micropore and

mesopore surface areas such as CX should lead to a decreased free citrate concentration when compared with Au-decoration processes that involve the use of CF, CB, or ND, which are mainly mesoporous materials. As this free-citrate concentration enables both the GNP growth and dispersion, the effect of this CX-citrate interaction might lead to the measured larger GNP diameters.

AC and OMC dramatically showed this effect. Their huge micropore area combined with mesopore areas of 602 and 94 m^2/g (Table 2), respectively, together with their poorer dispersibility in water resulted in even larger Au fcc average crystallite sizes (16.9 and 27.0 for OMC and AC, respectively) and the need of larger carbon support contents: both materials required up to 1:4 gold:carbon support w/w ratio to be able to allocate all GNP, which contrasts with the 1:1 and 1:2 gold:carbon support w/w ratios achieved for GO, and for carbon nanotubes, CB and ND, respectively (Fig. 3), highly mesoporous carbon supports whose BET surface areas are around 200-300 m^2/g (Table 2). Table 3 reveals that there is not a straightforward correlation between the gold content and the GNP size, therefore suggesting that both the structural and textural features of each carbon support used, together with, eventually, the presence of functional groups on their surface determine the obtained GNP size. The high gold contents of these gold-carbon hybrids (as high as 49 wt. % for Au-GO, Table 3) also accounts for the ability of these carbon supports for allocating GNP. The use of Au-AC and Au-OMC hybrids led to the lowest maximum conversion values (Fig. 3, Table 3). On the contrary, GO, that exhibits high microporosity, behaves here differently probably due to that the microporosity present in the dry solid drastically decreased when the material was highly exfoliated in water, leading to a huge surface area available for the GNP deposition. Moreover, the high oxygen-based functional group mainly as alcohol and epoxide groups [50] (44.9 wt. % O content, Table 1) allowed a

good GO dispersibility in water, so less citrate was required to interact with the GO surface, remaining free in solution to stabilize GNP. The presence of these oxygen-containing functional groups in GO and also in ND (mainly as alcohol groups [51], 9.6 wt. % O, Table 1) may also assist the GNP deposition and, eventually, may favor the gold-carbon hybrid/reactants interaction, so they may also further account for the enhanced catalytic performance of their hybrids. On the other hand, gold-carbon hybrid catalysts involving carbon supports that exhibited poor dispersibility in water and low BET surface areas such as G and GC required the largest carbon support contents (1:32 and 1:16, respectively) to provide their highest conversion values (Fig. 3). It is also worth mentioning that, in spite of the significant differences among the tested carbon supports in terms of structural and textural features, composition, dispersibility, and GNP size of the resulting hybrids, not quite large differences in the highest TON values have been measured. These differences might be even smaller if TON values are calculated considering the calculated mass balances for each gold-carbon hybrid composition. Fig. 4 shows that taking into account the number of moles of the reactants and the resulting product, mass balance values higher than 90% were achieved for low carbon support contents. As mentioned above, the addition of large support amounts ultimately leads to hindered reactants diffusion (the reaction volume was kept at 1 mL for all catalysis experiments). However, significant product adsorption on the carbon supports used might be expected, and this would more markedly occur when using carbon supports exhibiting high BET surface areas and well-developed microporosity (such as AC, OMC, and CX) and probably also in carbon supports with oxygen-containing functional groups (GO, ND). This might account for the mass balance values around 70% calculated for the corresponding gold-carbon hybrids (Fig. 4). At this point,

it is important to insist again that no by-products of the hydroamination reaction have been detected by ^{1}H NMR.

The kinetics of the reaction for the gold-carbon hybrids that provided the highest TON values were studied. Thus, Fig. 5 compares the conversion of phenylacetylene into phenyl-(1-phenylethilidene)amine in presence of Au-CB and Au-SWCNT 1:2 catalysts as a function of time. While both Au-CB and Au-SWCNT hybrids provided similar conversions (79 and 74 %, respectively, Table 4), the maximum conversion is reached faster when using CB as support, probably due to the presence of more active smaller nanoparticles in CB. Fig. 5 suggests that deactivation with time of the catalyst occurs. TEM characterization of the gold-carbon hybrids after reaction might indicate that catalyst deactivation can be addressed to GNP agglomeration (Fig. 6), accounting for the lack of cyclability of the synthesized gold-carbon hybrids for this catalytic application and, therefore, impeding catalyst reusability.

Finally, the catalytic performance of gold/carbon foams produced by laser ablation of chloro(triphenylphosphine)gold(I) ([$AuCl(PPh_3)$]) was evaluated (Fig. 7) [40,52]. This gold-carbon hybrid consists of GNP embedded within carbon matrices that comprise both amorphous carbon aggregates and graphitic nanostructures. Gold loading of 33 wt. % and average Au fcc crystallite size of 23.0 nm were measured by TGA and XRD, respectively. Contrary to the Au-CF hybrids produced by the GNP chemical decoration route described in this work, no catalytic activity has been however achieved with these gold/carbon foams. TEM characterization reveals that all observed GNP are coated with carbon layers (Fig. 7), that can eventually be extremely thin (Fig. 7, see insets). This would prevent the required interaction between the catalyst and the reactants, therefore accounting for the lack of catalytic activity of this gold-carbon

hybrid. This result highlights the convenience of the GNP decoration chemical route described here for the efficient application of CF in catalysis.

4. Conclusions

Gold-carbon hybrids can efficiently be used for the catalysis of the hydroamination reaction of phenylacetylene with aniline. Our results clearly indicate that the carbon support structure, composition, dispersibility, and porosity greatly affect the GNP decoration process and the resulting GNP size and, therefore, the catalytic performance of the gold-carbon hybrids. The best gold-carbon hybrid catalyst performance in terms of conversion values and low carbon support content has been achieved when using GO as well as supports that combine high BET surface areas, well-developed mesoporosity, and good dispersibility in water during the GNP decoration process (CB, SWCNT, MWCNT, and ND). However, remarkable catalyst performance can be eventually achieved for all tested carbon supports when suitably adjusting the gold:carbon support w/w ratios. We believe that improved catalyst performance may be achieved by further optimizing the GNP deposition process as well as the gold loading for the reaction volume used, which in turn are key issues toward commercial applications for these gold-carbon catalysts. Future work on the way to the practical use of these hybrids will be focused in exploring the catalysis of other organic reactions, as well as in enhancing the catalysis performance in terms of conversion and catalyst cyclability and lifetime through further tailoring the GNP size and the carbon support (for example, by means of support- [19,22,39,40,53-58] and GNP [16] functionalization) to prevent GNP leaching and the observed GNP agglomeration.

Acknowledgements

This work has been supported by the regional Government of Aragón (Spain, Project PI119/09, and Research Groups funding). This work has been funded in part by the European Commission through projects FP7 Grant agreement # 280658 and LIFE11/ENV/ES 560. The authors would like to acknowledge the use of Servicio de Microscopia Electrónica (Servicios de Apoyo a la Investigación), Universidad de Zaragoza. The authors also thank the technical assistance and characterization studies provided by all sections of the Analysis Service of the Instituto de Carboquímica ICB-CSIC. CB and AC samples were kindly supplied by Delta Tecnic S.A. and Morgui Clima S.L, respectively.

REFERENCES

[1] L. Calvillo, M.J. Lázaro, E. García-Bordejé, R. Moliner, P.L. Cabot, I. Esparbé, E. Pastor, J.J. Quintana, J. Power Sources 169 (2007) 59-64.

[2] M. Sevilla, C. Sanchos, T. Valdés-Solís, E. Murallón, A.B. Fuertes, Electrochim. Acta 54 (2009) 2234–2238.

[3] N. Tsiouvaras, M.V. Martínez-Huerta, R. Moliner, M.J. Lázaro, J.L. Rodríguez, E. Pastor, M.A. Peña, J.L.G. Fierro, J. Power Sources 186 (2009) 299-304.

[4] E. Lafuente, E. Muñoz, A.M. Benito, W.K. Maser, M.T. Martínez, F. Alcaide, L. Ganborena, I. Cendoya, O. Miguel, J. Rodríguez, E.P. Urriolabeitia, R. Navarro, J. Mater. Res. 21 (2006) 2841-2846.

[5] C. Moreno-Castilla, F.J. Maldonado-Hódar, Carbon 43 (2003) 455-465.

[6] S. Guo, X. Pan, H. Gao, Z. Yang, J. Zhao, X. Bao, Chem. Eur. J. 16 (2010) 5379–5384.

[7] A. Corma, H. Garcia, A. Leyva, J. Mol. Catal. A 230 (2005) 97–105.

[8] M. Cano, A. Benito, W.K. Maser, E.P. Urriolabeitia, Carbon 49 (2011) 652-658.

[9] M.B. Dawidziuk, F. Carrasco-Marín, C. Moreno-Castilla, Carbon 47 (2009) 2679-2687.

[10] D.A. Giljohann, D.S. Seferos, W.L. Daniel, M.D. Massich, P.C. Patel, C.A. Mirkin, Angew. Chem. Int. Ed. 49 (2010) 3280–3294

[11] A. Corma, H. García, Chem. Soc. Rev. 37 (2008) 2096–2126.

[12] R. Grisel, K.J. Weststrate, A. Gluhoi, B.E. Nieuwenhuys, Gold Bull. 35 (2002) 39-45.

[13] M. Haruta, Catal. Today 36 (1997) 153-166.

[14] A.S.K. Hashmi, G.J. Hutchings, Angew. Chem. Int. Ed. 45 (2006) 7896–7936.

[15] M. Haruta, Chem. Rec. 3 (2003) 75-87.

[16] H. Huang, Y. Zhou, H. Liu, Beilstein J. Org. Chem. 7 (2011) 897-936.

[17] J. Huang , L. Zhang, B. Chen, N. Ji, F. Chen, Y. Zhang, Z. Zhang, Nanoscale 2 (2010) 2733-2738.

[18] E.G. Rodrigues, S.A.C. Carabineiro, J.J. Delgado, X. Chen, M.F.R. Pereira, J.J.M. Órfão, J. Catal. 285 (2012) 83-91.

[19] J. John, E. Gravel, A. Hagège, H. Li, T. Gacoin, E. Doris, Angew. Chem. Int. Ed. 50 (2011) 7533-7536.

[20] Y. Li, X. Fan, J. Qi, J. Ji, S. Wang, G. Zhang, F. Zhang, Mater. Res. Bull. 45 (2010) 1413-1418.

[21] R. Martin, S. Navalon, J.J. Delgado, J.J. Calvino, M. Álvaro, H. Garcia, Chem. Eur. J. 17 (2011) 9494-9502.

[22] V. Tzitzios, V. Georgakilas, E. Oikonomou, M. Karakassides, D. Petridis, Carbon 44 (2006) 848-853.

[23] G.M.A. Rahman, D.M. Guldi, E. Zambon, L. Pasquato, N. Tagmatarchis, M. Prato, Small 1 (2005) 527-530.

[24] B. Wu, Y. Kuang, X. Zhang, J. Chen, Nano Today 6 (2011) 75-90.

[25] Y.H. Jang, S.T. Kochuveed, Y.J. Jang, H.Y. Shin, S. Yoon, M. Steinhart, D.H. Kim, Carbon 49 (2011) 2120–2126.

[26] D. Du, W. Chen, W. Zhang, D. Liu, H. Li, Y. Lin, Biosens. Bioelectron. 25 (2010) 1370-1375.

[27] S.J. Henley, P.C.S. Watts, N. Mureau, S.R.P. Silva, Appl. Phys. A 93 (2008) 875-879.

[28] R. Zhang, M. Hummelgard, H. Olin, Mat. Sci. Eng. B 158 (2009) 48-52.

[29] N. Hermanns, S. Dahmen, C. Bolm, S. Bräse, Angew. Chem. Int. Ed. 41 (2002) 3692-3694.

[30] R.A. Widenhoefer, X. Han, Eur. J. Org. Chem. 20 (2006) 4555-4563.

[31] T.E. Müller, K.C. Hultzsch, M. Yus, F. Foubelo, M. Tada, Chem. Rev. 108 (2008) 3795–3892.

[32] S. Hummel, S.F. Kirsch, Beilstein J. Org. Chem. 7 (2011) 847–859.

[33] P. Nun, S. Dupuy, S. Gaillard, A. Poater, L. Caravallo, S.P. Nolan, Catal Sci Technol. 1 (2011) 56-61.

[34] H. Ito, T. Harada, H. Ohmiya, M. Sawamura, Beilstein J. Org. Chem. 7 (2011) 951–959.

[35] A. Corma, P. Concepción, I. Domínguez, V. Forné, M.J. Sabater, J. Catal. 251 (2007) 39-47.

[36] P. Nikokaev, M.J. Bronikowski, R.K. Bradley, F. Rohmund, D.T. Colbert, K.A. Smith, R.E. Smalley, Chem. Phys. Lett. 313 (1999) 91-97.

[37] W.S. Hummers, R.E. Offeman, J. Am. Chem. Soc. 80 (1958) 1339.

[38] A. Krisnan, E. Dujardin, M.M.J. Treacy, J. Hugdahl, S. Lynum, T.W. Ebbesen, Nature 388 (1997) 451-454.

[39] C. Alegre, L. Calvillo, R. Moliner, J.A. González-Expósito, O. Guillén-Villafuerte, M.N. Martínez Huerta, E. Pastor, M.J. Lázaro, J. Power Sources 196 (2011) 4226-4235.

[40] E. Muñoz, M.L. Ruiz-González, A. Seral-Ascaso, M.L. Sanjuán, J.M. González-Calbet, M. Laguna M, G.F. de la Fuente, Carbon 48 (2010) 1807-1814.

[41] J. Kimling, M. Maier, B. Okenve, V. Kotaidis, H. Ballot, A. Plech, J. Phys. Chem. B 110 (2006) 15700-15707.

[42] S.K. Sivaraman, S. Kumar, V. Santhanam, Colloid Interf. Sci. 361 (2011) 543-547.

[43] N.R. Jana, L. Gearheart, C.J. Murphy, Langmuir 17 (2001) 6782-6786.

[44] M. Brust, M. Walker, D. Bethell, D.J. Schiffrin, R. Whyman, J. Chem. Soc. Chem. Comm. (1994) 801-802.

[45] P.C. Lee, D. Maisel, J. Phys. Chem. 86 (1982) 3391-3395.

[46] X. Liu, M. Atwater, J. Wang, Q. Huo, Coll. Surf. B: Bioint. 58 (2007) 3-7.

[47] C. Suryanarayana, M. Grant Norton, X-ray diffraction: a practical approach, first ed., Plenum Press, first ed., New York, 1998.

[48] J. Zhang, D. Su, A. Zhang, D. Wang, R. Schlögl, C. Hébert, Angew. Chem. Int. Ed. 46 (2007) 7319-7323.

[49] L. Bardotti, B. Prével, P. Jensen, M. Treilleux, P. Mélinon, A. Perez, J. Gierak, G. Faini, D. Mailly, Appl. Surf. Sci. 191 (2002) 205-210.

[50] D. R. Dreyer, S. Park, C. W. B. Rodney, S. Ruoff, Chem. Soc. Rev. 39 (2010) 228-240.

[51] M. Dubois, K. Guérin, N. Batisse, E. Petit, A. Hamwi, N. Komatsu, H. Kharbache, P. Pirotte, F. Masin, Solid State Nuc. Mag. 40 (2011) 144–154.

[52] E. Muñoz, M. de Val, M.L. Ruiz-González, C. López-Gascón, M.L. Sanjuán, M.T. Martínez, M. Laguna, G.F. de la Fuente, Chem. Phys. Lett. 420 (2006) 86-89.

[53] Y. Cao, R. Yuan, Y. Chai, L. Mao, H. Niu, H. Liu, Y. Zhuo, Biosens. Bioelectron. 31 (2012) 305-309

[54] J.A. Tang, D.P. Tang, B.L. Su**,** J. Huang, B. Qiu, G. Chen, Biosens. Bioelectron. 26 (2011) 3219-3226.

[55] X. Hou, L. Wang, X. Wang, Z. Li, Diamond Relat. Mater. 20 (2011) 1329-1332.

[56] N. Li, Q. Xu, M. Zhou, W. Xia, X. Chen, M. Bron, W. Schuhmann, M. Muhler, Electrochem. Comm. 12 (2010) 939-943.

[57] Y. Gu, X. Hou, H. Hu, B. Yu, L. Wang, F. Zhou, Mater. Chem. Phys. 116 (2009) 284-288.

[58] D. Sebastián, J.C. Calderón, J.A. González-Expósito, E. Pastor, M.V. Martínez-Huerta, I. Suelves I, R. Moliner, M.J. Lázaro, Int. J. Hyd. Ener. 35 (2010) 9934-9942.

Table 1
Elemental composition of the tested carbon supports.

Material	O %	C %	H %	N %	S %
SWCNT	1.4	76.4	0.4	0.2	0.0
MWCNT	0.2	99.2	0.0	0.1	0.0
GO	44.9	44.6	2.5	0.2	0.6
CF	2.1	96.3	0.7	0.1	0.0
GC	0.1	99.3	0.4	0.7	0.0
CB	0.2	98.6	0.0	0.2	0.0
G	0.6	96.9	0.0	0.1	0.0
CX	2.5	92.6	1.3	0.2	0.0
ND	9.6	83.7	0.7	2.6	0.0
AC	5.9	87.9	0.8	0.2	0.0
OMC	7.7	82.6	2.1	0.2	0.0

Table 2
Textural properties of the tested carbon supports.

Carbon support	BET surface area[a] (m^2/g)	Mesopore area[b] (m^2/g)	Mesopore volume[c] (cm^3/g)	Micropore area[d] (m^2/g)	Micropore volume[e] (cm^3/g)
SWCNT	298	284	0.975	-	-
MWCNT	171	220	0.897	-	-
GO	169	11	0.008	161	0.094
CF	63	64	0.168	-	-
GC	26	26	0.069	-	-
CB	204	125	0.329	38	0.015
G	8	11	0.039	-	-
CX	515	261	1.461	260	0.140
ND	341	437	1.031	-	-
AC	754	94	0.082	703	0.412
OMC	912	602	0.472	863	0.525

[a] Surface area of the carbon supports measured by the BET method, between 0.05 and 0.3 P/P_0.
[b] BJH desorption cumulative area of pores between 1.7 and 300 nm.
[c] BJH desorption cumulative volume of pores between 1.7 and 300 nm.
[d] Micropore area measured by t-Plot method.
[e] Micropore volume measured by t-Plot method.

Table 3
Composition, average Au fcc crystallite size and conversion of the gold-carbon hybrids that provided the best catalytic performance for each carbon support used.

Carbon support	Gold-carbon hybrid composition	Gold loading (wt. %)	Average crystallite size (nm)	Conversion (%)	TON
SWCNT	1:2	28	9.2	74	35
MWCNT	1:2	34	11.7	74	29
GO	1:1	49	12.4	76	31
CF	1:4	21	6.7	68	26
GC	1:16	6	14.8	69	29
CB	1:2	33	5.4	79	32
G	1:32	3	14.1	69	27
CX	1:2	34	14.7	61	24
ND	1:2	33	5.7	69	28
AC	1:4	19	27.8	55	23
OMC	1:4	19	16.9	56	24

Figure Captions

Fig. 1. TEM images of SWCNT (a), GC (b), G (c) and GO (d) decorated with GNP.

Fig. 2. TEM micrographs of CN (a), CB (b), CF (c), OMC (d), CX (e) and AC (f) decorated with GNP.

Fig. 3. Conversion values achieved using gold-carbon hybrids at different gold:carbon support w/w ratios.

Fig. 3. Conversion values achieved using gold-carbon hybrids at different gold:carbon support w/w ratios (black and white version of Fig. 3).

Fig. 4. Mass balance for each tested synthesized gold-carbon hybrid after performing the targeted catalytic reaction.

Fig. 5. Kinetics of the studied catalytic reaction when using Au-CB (solid line) and Au-SWCNT (dotted line) 1:2 hybrids.

Fig. 6. TEM micrographs of Au-SWCNT hybrid after reaction showing large GNP agglomeration.

Fig. 7. TEM micrograph of gold/carbon foams produced by laser ablation of [$AuCl(PPh_3)$].

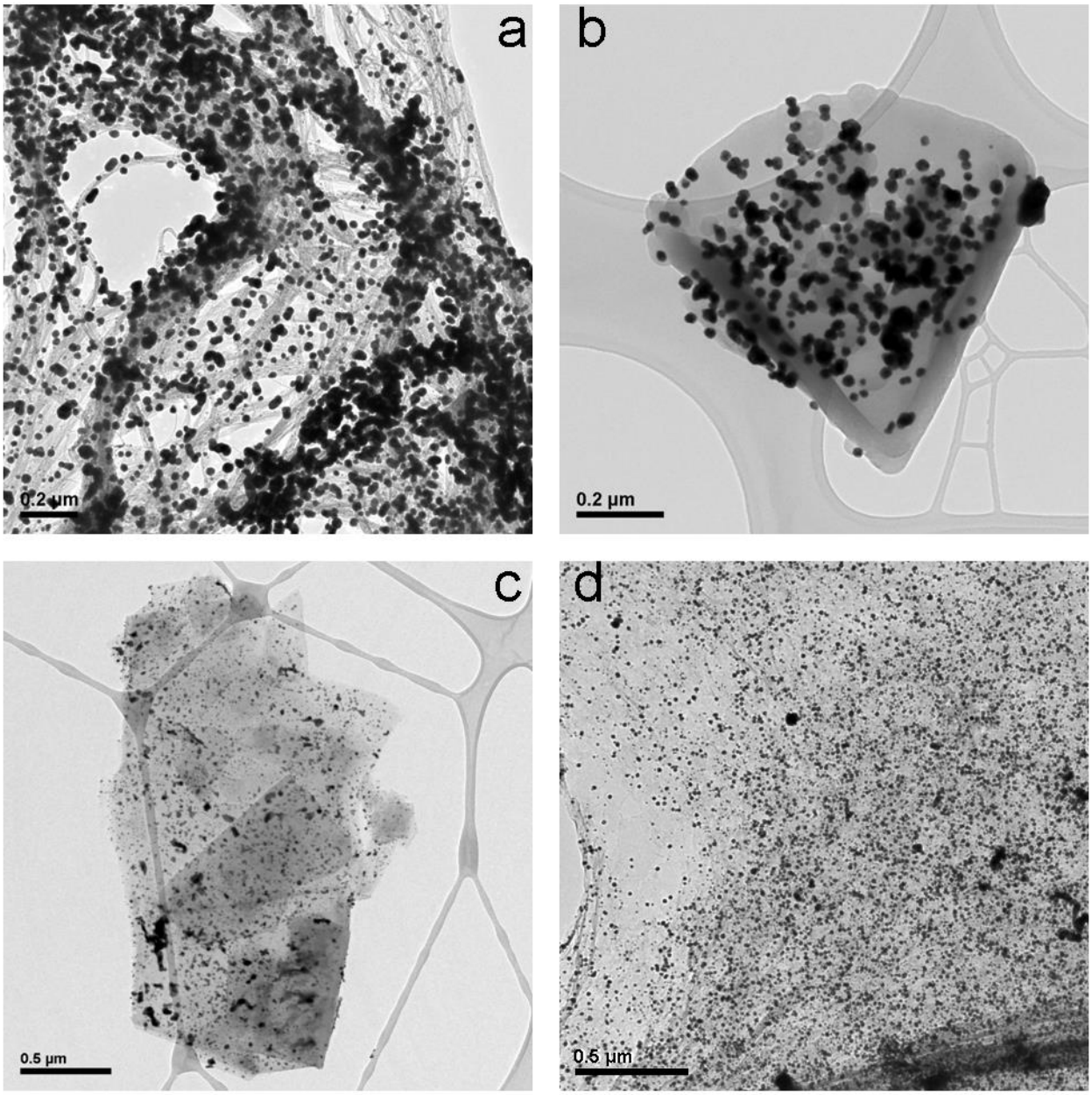

Fig. 1. TEM images of SWCNT (a), GC (b), G (c) and GO (d) decorated with GNP.

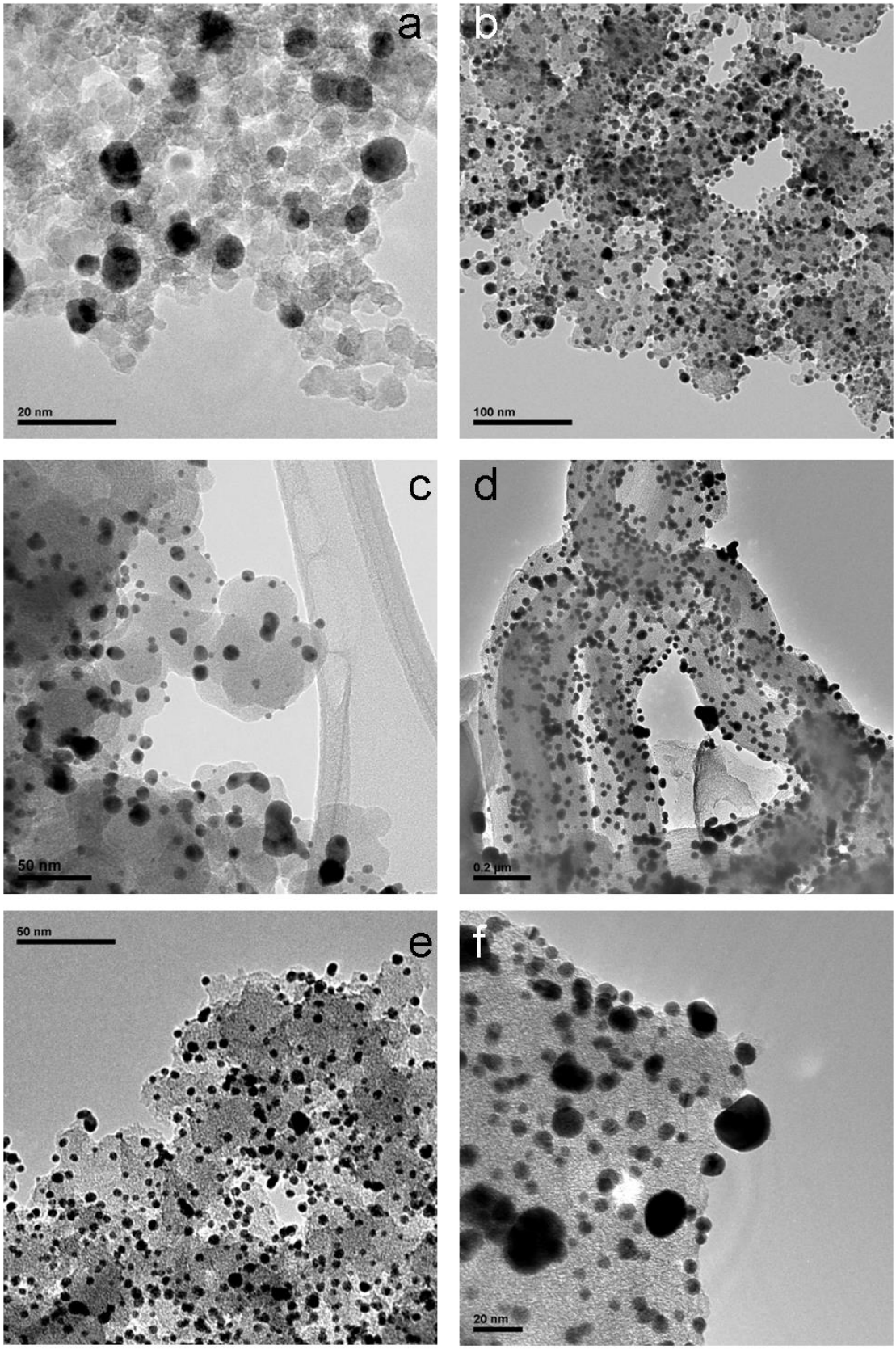

Fig. 2. TEM micrographs of CN (a), CB (b), CF (c), OMC (d), CX (e) and AC (f) supports decorated with GNP.

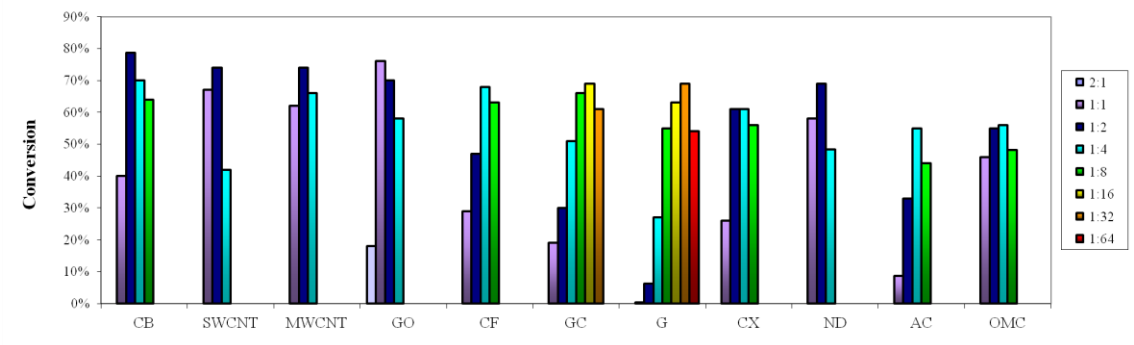

Fig. 3. Conversion values achieved using gold-carbon hybrids at different gold:carbon support w/w ratios.

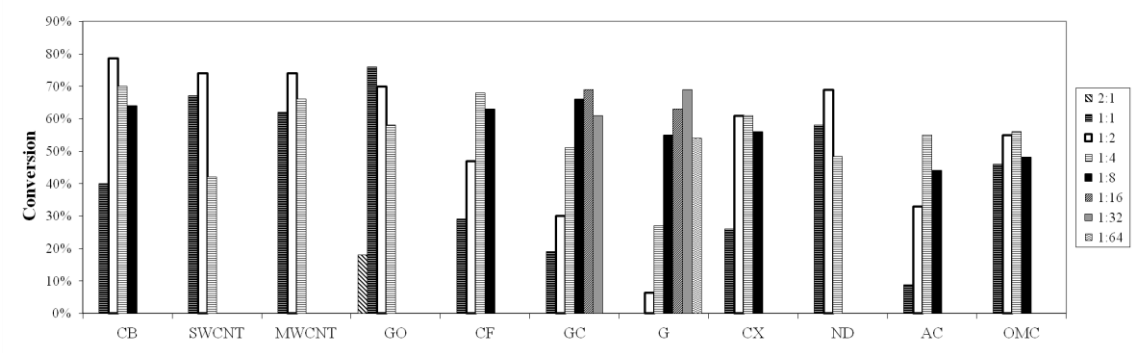

Fig. 3. Conversion values achieved using gold-carbon hybrids at different gold:carbon support w/w ratios (black and white version of Fig. 3).

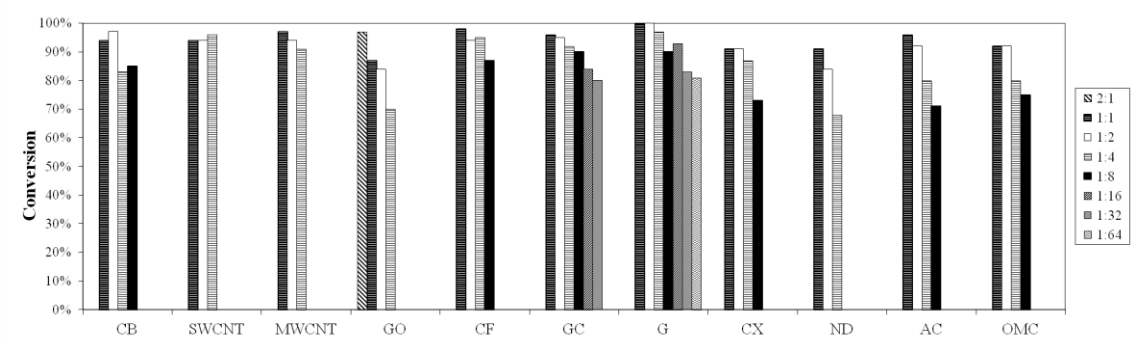

Fig. 4. Mass balance for each tested synthesized gold-carbon hybrid after performing the targeted catalytic reaction.

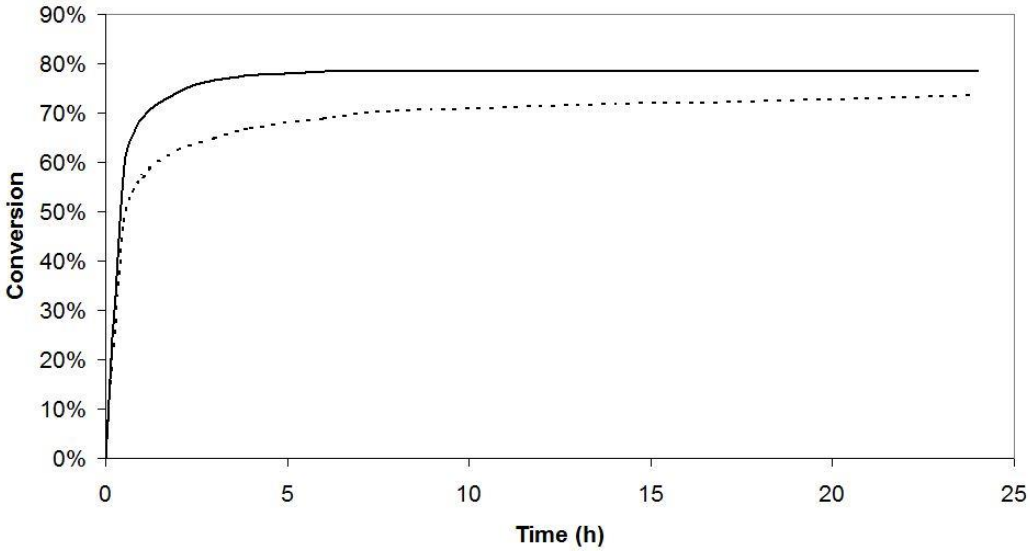

Fig. 5. Kinetics of the studied catalytic reaction when using Au-CB (solid line) and Au-SWCNT (dotted line) 1:2 hybrids.

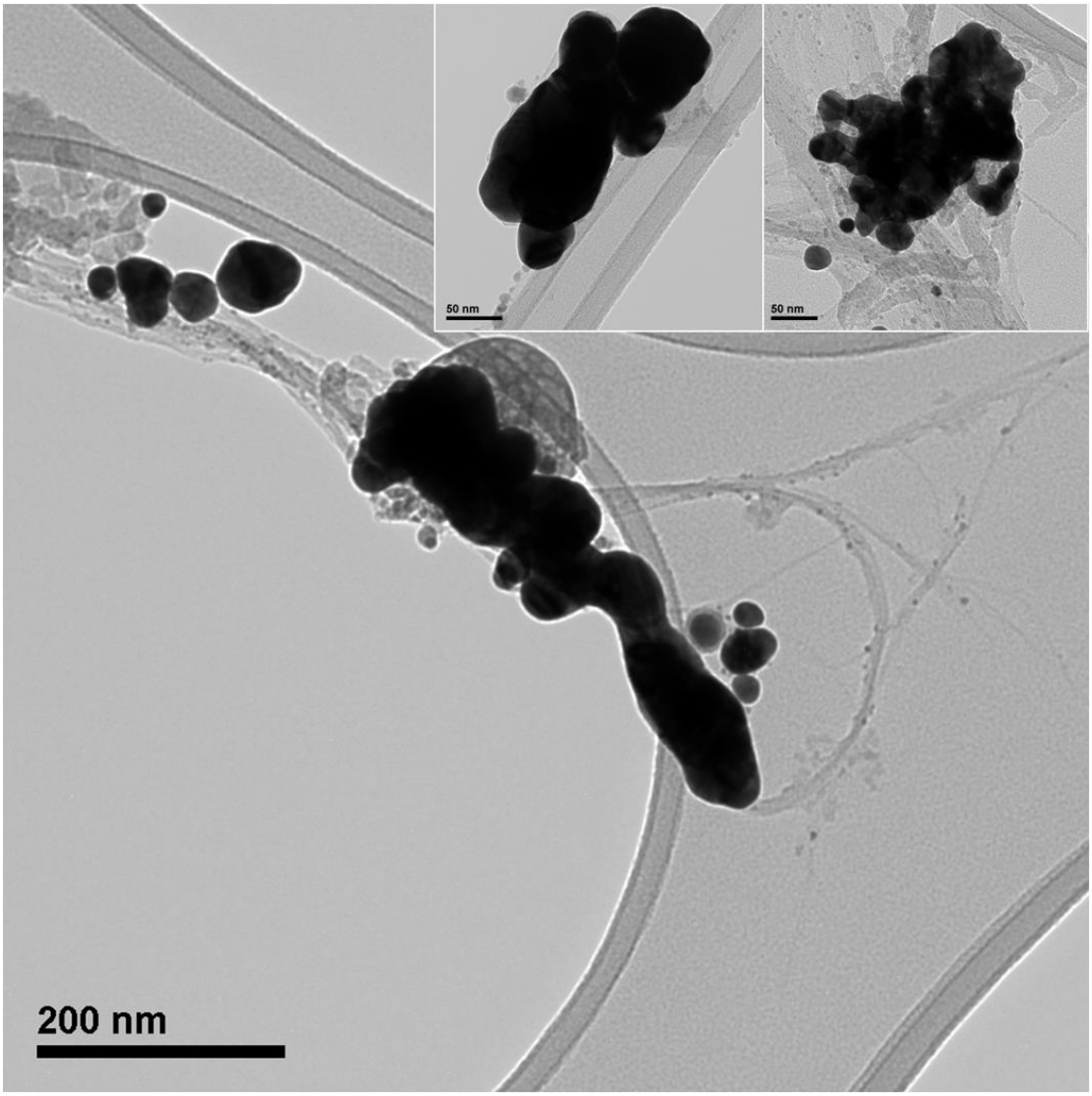

Fig. 6. TEM micrographs of Au-SWCNT hybrid after reaction showing large GNP agglomeration.

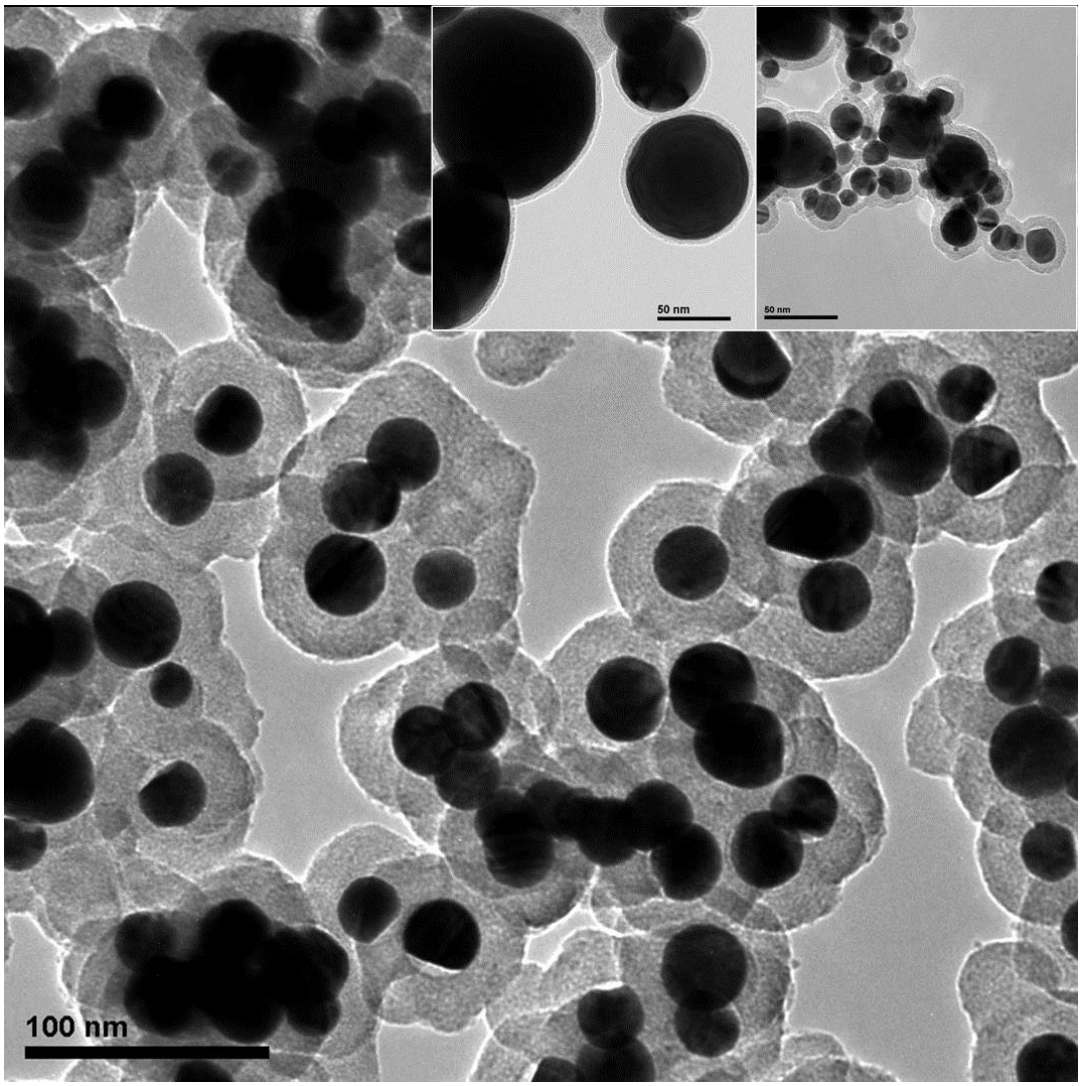

Fig. 7. TEM micrograph of gold/carbon foams produced by laser ablation of [AuCl(PPh_3)].